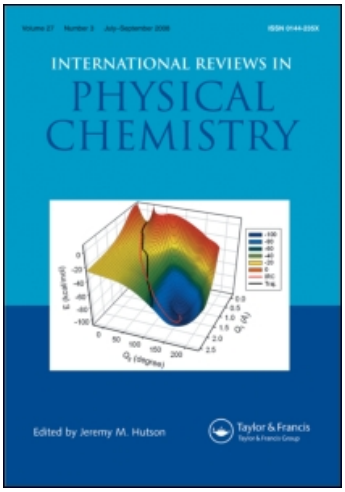

International Reviews in Physical Chemistry
Publication details, including instructions for authors and subscription information:
http://www.informaworld.com/smpp/title~content=t713724383

Heterogeneous chemistry in the troposphere: A modern surface chemistry approach to the study of fundamental processes

John C. Hemminger

Online publication date: 26 November 2010

To cite this Article Hemminger, John C.(1999) 'Heterogeneous chemistry in the troposphere: A modern surface chemistry approach to the study of fundamental processes', International Reviews in Physical Chemistry, 18: 3, 387 — 417
To link to this Article: DOI: 10.1080/014423599229929
URL: http://dx.doi.org/10.1080/014423599229929

INTERNATIONAL REVIEWS IN PHYSICAL CHEMISTRY, 1999, VOL. 18, NO. 3, 387–417

Heterogeneous chemistry in the troposphere: a modern surface chemistry approach to the study of fundamental processes

JOHN C. HEMMINGER

Department of Chemistry, University of California, Irvine, California 92697-2025, USA

There is an increasing amount of evidence that points to the importance of halogen chemistry in the troposphere in addition to the well known important chemistry in the stratosphere. Likely sources of halogens in the troposphere include reactions of gas phase pollutants with particles containing alkali halide salts such as sea salt particles. In this article we describe how modern ultra-high vacuum surface science experiments can provide significant new insight into the detailed mechanisms of reactions that are important to the chemistry of particles in the atmosphere. An introduction to what is known about the surface chemistry of NaCl is provided followed by a description of the experimental techniques. Studies from our laboratory that are described here have shown that the reaction of *dry* nitric acid with NaCl is self-limiting leading to a chemically inert surface that is covered with a layer of sodium nitrate. Our experiments also show that very low vapour pressures of water provide enhanced ionic mobility on the surface leading to a recrystallization of the nitrate layer and phase separation from the NaCl. This results in open areas of clean NaCl that are then available for further reaction. The reaction of water with NaCl surfaces which have been previously 'corroded' by reaction with nitric acid and water leads to the dissociative adsorption of water to form surface OH^- species. This is in stark contrast to the completely reversible adsorption of water on defect free NaCl surfaces. A model is also presented that is consistent with the information provided by the detailed ultra-high vacuum surface science experiments and explains the dependence of the reaction of nitric acid with NaCl on the nitric acid pressure.

Contents

International Reviews in Physical Chemistry ISSN 0144-235X print/ISSN 1366-591X online © 1999 Taylor & Francis Ltd
http://www.tandf.co.uk/JNLS/rpc.htm http://www.taylorandfrancis.com/JNLS/rpc.htm

1. Introduction

The existence of multiple phases of matter in the atmosphere is obvious. As a result the heterogeneous nature of the chemistry of the atmosphere has always been abundantly clear. However, recently the processes that lead to particle formation and the tremendously important chemistry that occurs at the interface between phase boundaries has received increased attention. The recognition of the importance of the surface chemistry of stratospheric cloud particles to the processes which control ozone depletion in the polar stratosphere has resulted in an increased awareness of the potential importance of gas–solid interactions and surface reactions in atmospheric processes. The impact that particles in the troposphere have on the physical and radiative balance aspects of the atmosphere, has been the object of study for many years (Evelyn 1661, Finlayson-Pitts and Pitts 1986). However, recently there has been a much broader recognition of the potential importance of reactive chemistry that can occur involving molecules from the gas phase adsorbed onto the surfaces of tropospheric particles. It is now abundantly clear that the chemical 'processing' of gas phase constituents of the atmosphere via reactions on particle surfaces can play a significant role in the determination of the gas phase composition.

During the last 35 years, there has been tremendous progress in the development of new ultra-high vacuum (UHV) based experimental techniques for the study of the structure and reactivity of highly characterized solid surfaces. A major challenge in the application of modern UHV based experimental methods to problems in atmospheric chemistry is the high pressure and high relative humidity conditions that are relevant to the atmosphere. These methods have been successfully applied to the development of a fundamental molecular level understanding of processes that control such diverse areas of chemistry as catalysis, semiconductor processing, corrosion, tribology, and even the behaviour of medical implants. In many of these areas the same questions of a 'pressure gap' between UHV experiments and 'relevant' conditions exist. In spite of this challenge, modern UHV experimental methods have provided significant new insight into the fundamental processes that control how a catalytic process works, how to process semiconductors to produce electronic devices, how to control corrosion and how to optimize lubrication systems. This is in spite of the fact that the 'pressure gap' and associated phenomena are still debated in the catalysis literature.

The success of modern UHV experimental methods in these diverse areas of chemistry, comes from the fact that once fundamental underlying phenomena are understood, they can be used to create models under conditions applicable to a particular situation. An added dimension to the experimental complexity of atmospheric chemistry problems is the importance of highly reactive gas phase species such as radicals and other short lived compounds. While this adds to the experimental

challenges facing applications of modern surface science experiments in atmospheric chemistry the issues are not prohibitive. In a number of laboratories around the world the well established approach of modern UHV surface science is being applied to problems of importance in the stratosphere and the troposphere.

The emphasis of this article is on the troposphere with specific emphasis on the fundamental chemistry and surface structural processes that control the chemistry of sea salt particles in the marine troposphere.

1.1. *Sea salt particles in the troposphere*

There are several established sources of alkali halide containing particles in the troposphere. Among these are: ocean wave action that generates aerosols that can solidify as they are transported inland to regions of lower relative humidity (Woodcock 1953, 1972, Blanchard 1985, Ikegani *et al.* 1994, Gong and Barne 1997, Gong *et al.* 1997, O'Dowd *et al.* 1997), oil well fires in regions such as Kuwait where mixing of brine with the oil resulted in the aspiration of salt particulates in the resulting smoke, some volcanic eruptions such as El Chichon, as well as wind erosion of naturally occurring salt flats (Woods and Chuan 1983, Woods *et al.* 1985, Cahill *et al.* 1992, Cofer *et al.* 1992, Ferek *et al.* 1992, Parungo *et al.* 1992, Sheridan *et al.* 1992, Daum *et al.* 1993, Lowenthal *et al.* 1993, Stevens *et al.* 1993, Reid *et al.* 1994, Hebestrect *et al.* 1998).

While it would be expected that the sea salt particles in the tropospheric marine boundary layer (MBL) would have a Cl/Na ratio that is typical of sea water, it was observed as early as 1956, that sea salt particles collected in polluted marine areas showed a deficit of chloride and bromide relative to sodium (Junge 1956, Moyers and Duce 1972, Keene *et al.* 1990, Mouri and Okada 1993, McInnes *et al.* 1994). It has been assumed that such halogen deficits are the result of processing of the particles via reactions with gas phase pollutants such as nitric and sulphuric acid as well as other oxides of nitrogen. The known relevant reactions are:

$$NaCl(s) + HNO_3(g) \rightarrow NaNO_3(s) + HCl(g) \quad (1)$$

$$2NaCl(s) + H_2SO_4(g) \rightarrow Na_2SO_4(s) + 2HCl(g) \quad (2)$$

$$NaCl(s) + N_2O_5(g) \rightarrow NaNO_3(s) + ClNO_2(g) \quad (3)$$

$$NaCl(s) + 2NO_2(g) \rightarrow NaNO_3(s) + NOCl(g) \quad (4)$$

$$NaCl(s) + ClONO_2(g) \rightarrow NaNO_3(s) + Cl_2(g) \quad (5)$$

The result of the processing of sea salt particles by these reactions with gas phase atmospheric constituents is the observed depletion of halogen in the particles with the presumed liberation of halogenated gas phase species into the marine troposphere. Consistent with reactions (1)–(5) Posfai *et al.* (1995) using transmission electron microscopy (TEM) and X-ray fluorescence have observed $NaNO_3$ crystallites in collected sea salt particles.

The subsequent photochemical reactions of the halogenated products may have substantial impact on the chemistry of hydrocarbons as well as ozone in the troposphere as discussed in detail in the article by Finlayson-Pitts and co-workers in this issue (DeHaan *et al.* 1999). The relative implications of the reactions listed above to tropospheric chemistry depends on the stability of HCl relative to the photochemically active products of reactions (3)–(5) which would ultimately be a source of

Cl atoms in the troposphere. In order to consider including these halogen sources in any model of tropospheric chemistry one needs to know the detailed rates and mechanisms of these reactions.

Reactions (1)–(5) are all of the form that one solid and one gas phase product are produced. This is not an uncommon result of gas–solid reactions and is typical for example of corrosion reactions of metal surfaces. An extremely important detail in such situations is whether the solid product (in this case either $NaNO_3$(s) or Na_2SO_4(s)) forms a dense layer covering the solid thus resulting in a poisoning of the reaction and passivation of the surface or if there exists a mechanism for the reaction to continue in the presence of the product. Indeed, if in the case of interest here, a few molecular layers of the nitrate or sulphate were sufficient to passivate the NaCl surface, reactions (1)–(5) could not explain the observed Cl depletion and other depletion mechanisms, including possible aqueous phase chemistry in deliquesced droplets, would have to be considered. As will be discussed in detail in this article, this is an extremely important and interesting issue for these reactions.

The experimental approach that we have used (the results of which are described in this article) has been to use modern UHV based surface spectroscopic and microscopic methods and highly controlled and characterizable samples to study the reactions of interest. Our aim is to elucidate the fundamental rates and mechanisms involved and to touch base with more conventional atmospheric chemistry laboratory based methods (e.g. Knudsen cell experiments, and flow reactor experiments) by developing an understanding of the fundamental processes involved.

2. Background on the surface structure and chemistry of NaCl and $NaNO_3$

2.1. *Structure of NaCl*

Solid NaCl is a highly crystalline ionic compound. The room temperature, atmospheric pressure stable structure of NaCl is a cubic structure which involves the interlacing of a face centred cubic arrangement of Cl^- ions with a face centred cubic arrangement of Na^+ ions. Pictures of the crystal structure of NaCl can be found in virtually every freshman chemistry or solid state physics textbook. The arrangement of ions in the NaCl structure is such that each Na^+ is surrounded by 6 Cl^- neighbours and each Cl^- is surrounded by 6 Na^+. Thus, the (100) plane of a NaCl single crystal consists of equal numbers of Na^+ and Cl^- ions. This plane is electrostatically neutral, and thus provides a stable termination plane for the bulk NaCl structure. One result of this fact is that a NaCl single crystal can be cleaved to expose low defect density surfaces of (100) orientation. He atom scattering (Benedek *et al.* 1983) and atomic force microscopy experiments (Meyer and Amer 1990a, b) indicate that the Na^+ and Cl^- ions in the NaCl(100) surface occupy positions which are consistent with the structure of a NaCl(100) plane in the bulk. In contrast the (111) plane of NaCl contains either all Na^+ ions or all Cl^- ions. Such an arrangement of ions in the termination layer of a bulk material would have a very large electrostatic energy. As a result, when a NaCl single crystal is cut in such a manner as to expose a surface with a macroscopic (111) orientation, the surface facets to expose a large number of microcrystalline planes at the surface, leading to a reduced surface free energy and also a very large number of surface defects. Most of the surface physics and chemistry experimental work on NaCl has utilized the well defined, easily prepared (see section 3 for more experimental details) NaCl(100) surface. In our work we have also carried out experiments with the (111) surface as a means of making comparisons between low and high defect density surfaces.

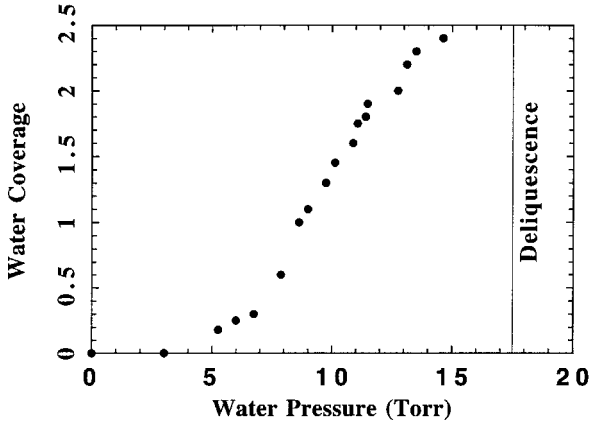

Figure 1. Adsorption isotherm for H_2O on NaCl(100) at 25 C (from Ewing and Peters (1997), with permission).

2.2. *Molecular adsorption and chemistry on NaCl(100)*

The reactivity of the surfaces of ionic and insulating surfaces tends to be much more mild than that of metal surfaces. The surface chemistry of NaCl(100) fits well with this categorization. As a result of experimental difficulties associated with the insulating NaCl sample, only a few molecular adsorption systems have been studied in detail on NaCl(100) surfaces. The molecular adsorption systems on NaCl(100) that have been studied in most detail, using modern UHV surface spectroscopies, include CO, CO_2, H_2O, and N_2O.

The adsorption of CO_2 and N_2O have been studied at low surface temperatures (77 K) (Weiss 1995). Under low surface temperature conditions, these adsorbates form molecular monolayers with two-dimensional ordering.

Ewing (1991) has carried out very complete studies of the adsorption and bonding of CO to NaCl(100) surfaces using infrared spectroscopy. As is the case with CO_2 and N_2O, CO adsorbs molecularly and reversibly on NaCl(100).

As will become evident later in this article, the interaction of H_2O with NaCl surfaces will be of great interest in our discussions of the reactions of nitrogen oxides with NaCl surfaces. The surface chemistry of H_2O on a variety of surfaces has been reviewed by Thiel and Madey (1987) and the adsorption of H_2O on NaCl(100) has been studied by a number of research groups utilizing photoelectron spectroscopy (Fölsch and Henzler 1991, Fölsch *et al.* 1992, Laux *et al.* 1994, 1996, Vogt *et al.* 1996), surface infrared spectroscopy (Ewing and Peters 1997), helium atom scattering (Bruch *et al.* 1995, Dai *et al.* 1995, Peters and Ewing 1997), and atomic force microscopy (Shindo *et al.* 1996, Xu *et al.* 1998). The most important aspects of the chemistry of H_2O on NaCl(100), as it applies to the topic of this article, are that it adsorbs molecularly on NaCl(100) surfaces that are held at low temperature, that the adsorption is essentially completely reversible when low defect density surfaces are used, and that adsorbed water enhances the mobility of steps on the surface when the sample is exposed to vapour pressures of water near the deliquescence point. When the surface is warmed in vacuum, the adsorbed water desorbs completely as molecular H_2O at temperatures of $\leqslant$ 150 K (Fölsch and Henzler 1991, Fölsch *et al.* 1992).

When a NaCl(100) surface, in vacuum, held at temperatures below 140 K, is exposed to H_2O vapour, a saturation molecular monolayer is formed. As a result of the molecular arrangement in this layer it is often referred to as a bilayer structure. The

same structure is observed for molecular water adsorption on many metal surfaces (Thiel and Madey 1987). Electronic structure calculations (periodic Hartree–Fock) for water adsorbed on NaCl(100) indicate that the bilayer structure is expected to be stable (Taylor *et al.* 1998). In the case of adsorption on very low defect density NaCl(100), when the surface is warmed in vacuum, the adsorbed water desorbs completely as molecular H_2O at temperatures of $\leqslant 150$ K (Fölsch and Henzler 1991, Fölsch *et al.* 1992). Indeed, experiments in our laboratory in which room temperature samples of NaCl(100) have been exposed to high pressures of H_2O (e.g.10 Torr) followed by evacuation to ultra high vacuum show that even under these extreme exposure conditions no residual or decomposed water remains on the surface immediately after pumping down to UHV conditions.

In contrast to the behaviour of water on low defect density NaCl(100) surfaces, adsorption of H_2O onto surfaces with defects can lead to dissociation to form OH^- surface species. Ewing and co-workers (Dai *et al.* 1995) used infrared spectroscopy to identify OH^- as the species that is formed from the dissociation of adsorbed H_2O at surface defects. Ultraviolet photoelectron spectroscopy has also been used to show that H_2O dissociates to form OH^- at f-centres on NaCl (Fölsch and Henzler 1991). Barnett and Landman (1996) used electronic structure calculations to investigate the dissociation of H_2O on small clusters of NaCl. Wasserman *et al.* (1993) have reported observing water adsorbed on NaCl at room temperature in second harmonic generation experiments. This observation is most likely explained by the fact that they used polished samples which are likely to have more defects than cleaved surfaces.

Adsorption isotherms for H_2O vapour exposed to NaCl(100) have been reported in the literature (Barraclough and Hall 1974, Ewing and Peters 1997). Figure 1 shows the adsorption isotherm for NaCl(100) at 298 K. At 298 K the first monolayer of adsorbed water is completed at a water vapour pressure of ~ 5 Torr. Above 7.5 Torr water vapour pressure multilayers of water are formed. The deliquescence point of NaCl at 298 K is ~ 17.5 Torr.

2.3. *Surface chemistry of $NaNO_3$*

Unfortunately, very few detailed experiments have been carried out on the surfaces of $NaNO_3$. This is most likely due to the difficulty in obtaining high quality $NaNO_3$ samples. The bulk crystal structure of $NaNO_3$ is rhombohedral. The deliquescence point of bulk $NaNO_3$, at 298 K, is $\sim 75\%$ (similar to NaCl). Knutsen and Orlando have reported studies of electron stimulated desorption of H^+, OH^-, O^+, and NO^+, from $NaNO_3$ crystals which were grown from aqueous solutions.

3. Experimental methods

In our experiments, which are described in detail in this article, we have utilized a combination of X-ray photoelectron spectroscopy (XPS) and transmission electron microscopy (TEM) to study the reaction of HNO_3 on NaCl(100) and the effect of H_2O on that chemistry.

The NaCl samples were purchased as large single crystals ($0.5\ cm \times 0.5\ cm \times 5.0$ cm) (purchased from Bicron). NaCl(100) samples that were ~ 1–2 mm thick were cleaved from these crystals in air, mounted on a sample holder that allowed temperature control and measurement (Lindquist and Hemminger, 1987) and immediately placed in the UHV chamber via a fast entry chamber. XPS experiments carried out on the samples immediately after introduction into the chamber typically showed no surface impurities. In some cases a small amount of carbon impurity was

observed. Heating of the samples to above 500 K prior to experiments did not change the subsequent HNO_3 surface chemistry. In particular it is important to note that there is no indication of any strongly bonded oxygen containing species on the freshly prepared NaCl(100) surface under our sample preparation conditions.

3.1. *X-ray photoelectron spectroscopy*

XPS has been used in our experiments to establish the composition of the NaCl(100) surface prior to exposure to reactive gases and to quantify the surface Cl^- and NO_3^- surface species as a function of exposure of the sample to gas phase HNO_3, and H_2O. An ESCALAB MkII photoelectron spectrometer (VG Scientific) was used in these experiments. The ESCALAB MkII is a multi-technique surface analysis instrument based on an UHV system consisting of three separately pumped, interconnected chambers that we refer to as the spectroscopy, sample preparation and fast entry chambers. The sample is easily moved from one chamber to the other under UHV conditions with temperature control capabilities in both the spectroscopy and sample preparation chambers. The XPS experiments were performed in the spectroscopy chamber using a standard Al/Mg twin anode X-ray source and a 150 mm hemispherical electron energy analyser. For these experiments, an analyser pass energy of 20 eV and either Mg Kα X-rays (1253.6 eV), or Al Kα X-rays (1486.6 eV) were used. Base pressures in the spectroscopy chamber during XPS analysis were typically in the low-to-mid 10^{-10} Torr range.

XPS peak areas for N, Cl, O, and Na were measured after standard Shirley-type background subtraction. Standard XPS sensitivity factors for N, O and Cl (0.489, 0.721, 0.925 respectively, relative to the F sensitivity factor of 1.00) were used to quantify the surface concentrations of these elements (Wagner *et al.* 1981, Moulder *et al.* 1992). The XPS sensitivity factor for Na is not well established in the literature (Wagner *et al.* 1981), so we used a relative sensitivity factor of 3.8, developed for our instrument, which gives a Na:Cl ratio of 1:1 for freshly cleaved, clean NaCl.

3.2. *Nitric acid and water exposures*

Nitric acid exposures to the sample were carried out in the sample preparation chamber of the instrument to avoid contamination of the spectroscopy chamber with HNO_3. Water vapour exposures were carried out in the fast entry chamber to avoid cross contamination with residual HNO_3 in the sample preparation chamber. It is very difficult if not impossible to passivate a metal chamber or gas line towards HNO_3. Thus, dosing methods used in conventional surface chemistry studies are not appropriate to the quantitative exposure of nitric acid to a surface. An all glass capillary doser mounted on the preparation chamber, as shown in figure 2, allowed high doses of HNO_3 at the sample surface in a quantifiable manner without increasing the preparation chamber pressure substantially. The source of *dry* HNO_3 is the vapour above a HNO_3/H_2SO_4 50:50 v/v solution. The glass sample bulb is attached to the doser via a Teflon valve. The doser is attached to a standard 2.75 inch diameter stainless steel conflat flange via a glass-to-metal seal. A re-entrant glass tube makes it such that the HNO_3 does not come into contact with the metal of the flange or the glass to metal seal. At the end of the doser tube is a short segment of glass capillary tubing which has a conductance of 2×10^{-6} l s^{-1}. Thus, when there is 1 Torr of HNO_3 in the doser, 2×10^{-6} Torr l s^{-1} ($\sim 6.5\times 10^{13}$ molecules s^{-1}) of HNO_3 is delivered into the UHV chamber. The doser was passivated prior to actual experiments by running HNO_3 vapour through it for extended periods of time (usually overnight).

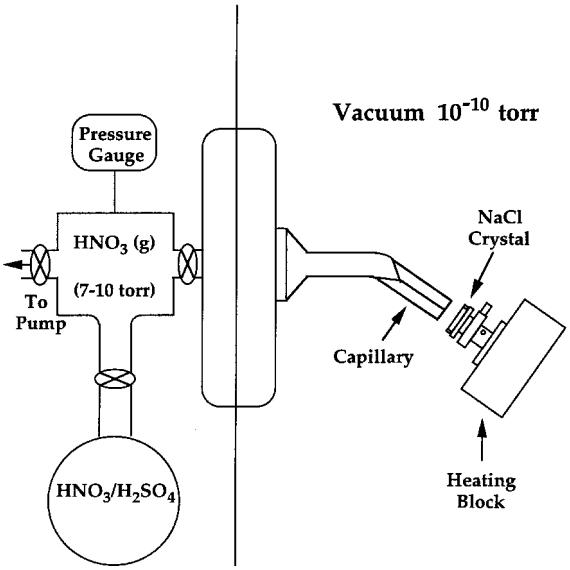

Figure 2. All glass dosing system for quantitative dosing of a sample under ultra high vacuum conditions with dry nitric acid vapour.

During dosing, the sample is placed within ~ 1 mm of the exit of the doser capillary. The angular distribution of molecules exiting the doser is difficult to calculate *a priori* (Yates 1998). However, by using a well studied gas phase adsorbate on a well studied surface (e.g. CO adsorption on Pt(111)) one can calibrate the fraction of gas molecules that directly strike the sample surface given the experimental geometry. For our experiments this fraction is ~ 50%. Experiments in which we checked the XPS signal levels as a function of lateral position on the sample showed that the dosing was reasonably uniform across the sample surface (variations of composition after dosing from edge to centre were less than 10%). The HNO_3 pressure behind the capillary was measured using a corrosion resistant capacitance manometer. Our experiments utilized 7 Torr or 10 Torr HNO_3 as the pressure behind the doser capillary. Comparisons of the experiments using 7 and 10 Torr HNO_3 pressures behind the capillary showed that the sample exposure scaled appropriately with HNO_3 pressures.

Exposure of the surface to water vapour was carried out in the fast entry chamber by bringing that whole chamber up to the desired H_2O pressure. A copper reservoir which could be filled with liquid nitrogen was added to the fast entry chamber to provide cryopumping of the water vapour. This was necessary to provide rapid pump down of the chamber at the end of an exposure so that the dosing time was well defined. At the end of a water dose, the valve to the water source was closed at the same time that the liquid nitrogen was added to the reservoir. This proved to be a very effective way to end the water dosing in a few seconds (typically 5–10 s) providing a well defined timing of the exposures.

3.3. *Transmission electron microscopy and energy dispersive analysis*

TEM and energy dispersive analysis (EDS) have been used to identify the changes in surface and bulk morphology as the chemistry of interest occurs. The TEM experiments were carried out at the UCI TEM facility using a Philips CM20 TEM (200 kV) with an EDS attachment (EDAX PV9800) for detection of X-ray fluorescence. In

the TEM experiments magnification of the sample ranged between 22× and 660 000×. Typical magnification used to locate and view micron size crystals ranged between 200× and 50 000×. To limit electron beam damage of the sample, a Gatan Cold Stage (Model 636-P1) which cooled the samples to liquid nitrogen temperatures was used during EDS spectra acquisition. Local heating due to the electron beam still occurred, however, the rate of beam induced heating of the sample was significantly reduced and therefore radiation damage was reduced to the point that reliable spectra could be obtained. A detailed study of the electron beam damage effects in these experiments has been published (Allen *et al.* 1998).

For the TEM experiments, sodium chloride crystals were grown from a 0.2 M NaCl solution on the Formvar side of a Pelco Carbon-Type B nickel TEM grid. In a typical experiment, three small droplets of the NaCl solution were initially placed on a Petri dish. Wiping of the grid over the droplets coalesced the drops underneath the Formvar coating. The grid was then allowed to 'float' on top of the solution at ~ 298 K until evaporation of the solution was complete (~ 30 min). Cubic sodium chloride particles in the micron size range were obtained by periodic agitation during the crystallization process.

Exposure of the NaCl crystals to nitric acid vapour as a mixture in He was carried out inside an all glass gas handling manifold. Water vapour exposures were carried out by exposure either to laboratory relative humidity (RH) and/or to the equilibrium vapour pressure above a reservoir of deionized water. Inside the all glass manifold, water vapour pressure was measured by two different Edwards high-vacuum pressure gauges (600 AB transducer 1000 Torr range with a Model 1500 electronic manometer and a 570 AB transducer 1000 Torr range with a Model 1174 electronic manometer). The laboratory relative humidity to which the sample was exposed was recorded by a Fisher Scientific humidity/temperature meter (Digital Tachometer™, Model 11-88-6), calibrated against the National Institute of Standards and Technology Traceable Instrumentation with a limit of error of ~ 1.5% RH and ±0.4 F.

For light element EDS analysis (< Na), a Phillips 420T transmission electron microscope (120 kV) with a Kevex/Fisons Light Element EDS attachment (Sigma LPX2) at the University of Southern California Center for Electron Microscopy and Microanalysis (CEMMA) was utilized.

4. Surface chemistry of dry HNO_3 on NaCl(100) and the effect of H_2O vapour

4.1. *The chemistry of dry HNO_3 with NaCl*(100)—*XPS results*

Figure 3 shows XPS spectra of the NaCl(100) sample before (figure 3 (*a*)) and after (figure 3 (*b*)) exposure to HNO_3. The spectrum shown in figure 3 (*b*) corresponds to a saturation exposure of HNO_3 to the sample as will be described in more detail below. The signals due to oxygen and nitrogen from the product of reaction 1 are easily observed. Figure 4 shows a higher resolution scan of just the N 1s region of the spectrum for several experiments with different HNO_3 exposure times. In each of the experiments, that generated the data shown in figure 4, the pressure of dry HNO_3 behind the capillary of the doser was 10 Torr. The binding energy scale has been corrected for a small amount of charging of the sample surface which occurs due to the insulating nature of the NaCl sample. The sample charging results in a shift of the entire spectrum by a few eV (typically 4–5 eV in these experiments). We correct for this effect by assigning a binding energy of 1072.0 eV to the Na 1s peak (Moulder *et al.* 1992). The binding energy of the N 1s peak is seen to be 407.8 eV. This is the expected 1s binding energy for the NO_3^- species (Moulder *et al.* 1992). In carrying out the

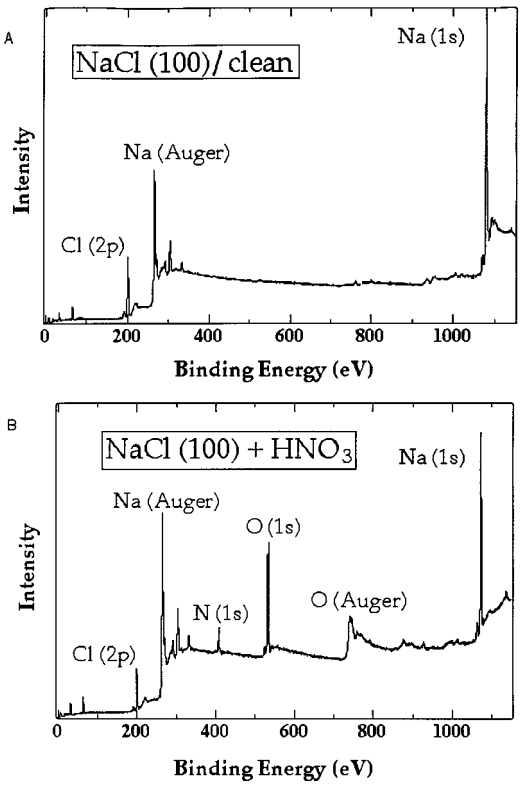

Figure 3. X-ray photoelectron survey spectra. (*a*) Clean NaCl(100). (*b*) NaCl(100) after exposure to a room temperature saturation dose of dry HNO_3.

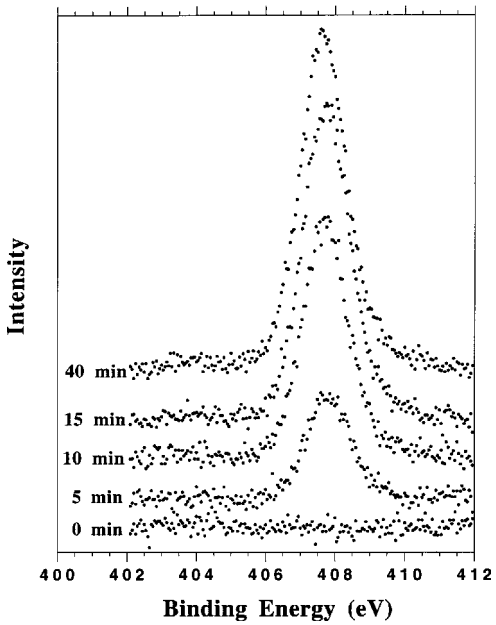

Figure 4. X-ray photoelectron N 1s spectra after dosing the NaCl(100) sample with dry HNO_3 for the indicated times with a 10 Torr pressure behind the doser capillary. The binding energies have been corrected for charging as indicated in the text.

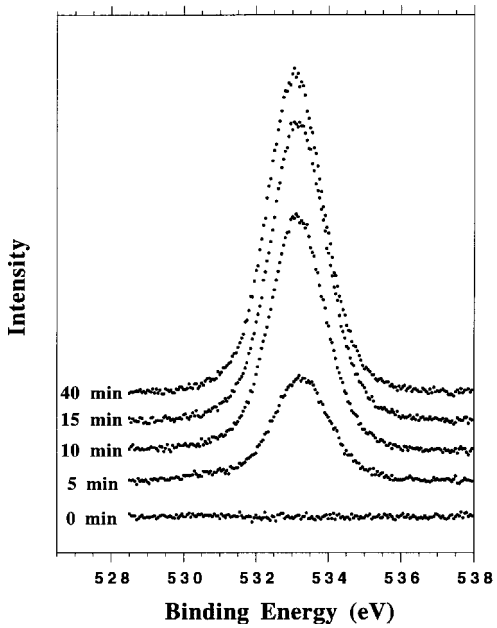

Figure 5. X-ray photoelectron O 1s spectra after dosing the NaCl(100) sample with dry HNO_3 for the indicated times with a 10 Torr pressure behind the doser capillary. The binding energies have been corrected for charging as indicated in the text.

experiments that resulted in the spectra of figure 4, care was taken to minimize the exposure of the sample to the X-rays. Extended X-ray irradiation of NaCl can generate f-centre defects in the sample. Also, extended X-ray irradiation of the $NaNO_3$ reaction product results in the formation of a nitrite (NO_2^-) surface species (Laux *et al.* 1994, 1996). The nitrite surface species is easily identified from the XPS spectra since the N 1s binding energy of the NO_2^- species is ~ 404 eV and thus it is easily seen as a separate peak in the N 1s region of the XPS spectrum (Laux *et al.* 1994, 1996, Vogt *et al.* 1996). Figures 5 and 6 show the O 1s region and the Cl 2p region of the XPS spectrum for the same set of experiments as in figure 4. The O 1s binding energy of 533.3 eV from these spectra is also consistent with a NO_3^- species (Moulder *et al.* 1992). The intensity of the Cl 2p peak (figure 6) decreases with increasing exposure since the surface is now being covered with the $NaNO_3$ layer. The Cl 2p spectrum is a doublet as expected due to spin–orbit splitting of the p state.

The surface composition of N, O and Cl relative to Na is obtained by measuring the areas under the appropriate photoelectron peaks and correcting these areas with the individual elements' sensitivity factors as described in the experimental section. Plots of the N, O and Cl relative to the surface Na are shown in figure 7, (*a*) as a function of HNO_3 exposure time for an experiment in which the pressure of dry HNO_3 behind the doser capillary was 10 Torr. Several things are immediately obvious from the data in figure 7(*a*). First the oxygen and nitrogen signals increase as a function of HNO_3 exposure and are in the ratio of O : N = 3 : 1 as would be expected for a NO_3^- species. Second, the changes in surface composition saturate after an exposure of ~ 20 min under these exposure conditions. This corresponds to approximately 4×10^{16} molecules having collided with the NaCl(100) surface (0.25 cm^2 surface area). The saturation behaviour of the signals as a function of dry HNO_3 exposure is consistent

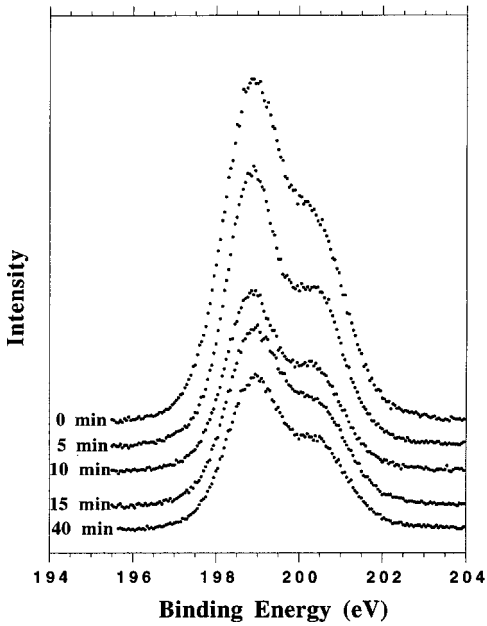

Figure 6. X-ray photoelectron Cl 2p spectra after dosing the NaCl(100) sample with dry HNO_3 for the indicated times with a 10 Torr pressure behind the doser capillary. The binding energies have been corrected for charging as indicated in the text.

with a picture in which the surface is covered with a passivating film of $NaNO_3$. Indeed, the decrease in the Cl 2p signal is due to the inelastic scattering of the Cl 2p photoelectrons as they traverse the $NaNO_3$ film to exit the sample. Assuming that the nitrate film is uniform, the decrease in the Cl signal can be used to estimate the thickness of the nitrate layer covering the NaCl(100) surface. The relationship between film thickness and the signal strengths with and without the $NaNO_3$ film is given by (6):

$$d = \lambda_L \ln [I_0/I_x], \tag{6}$$

where d is the nitrate layer thickness, λ_L is the attenuation length for a Cl 2p photoelectron in $NaNO_3$(s) (~ 2.1 nm) (Briggs and Seah 1990), I_0 is the Cl 2p peak area of the fresh NaCl crystal, and I_x is the Cl 2p peak area after saturation with HNO_3. Using this approach an estimate of 1–2 monolayers is obtained for the nitrate film thickness.

An average reactive sticking coefficient, ϕ (the number of HNO_3 molecules which react with the surface to form $NaNO_3$ divided by the total number that strike the surface), can be obtained from the dosage required for saturation film formation and the fact that the saturation nitrate film corresponds to the replacement of ~ 1 monolayer of Cl^- with NO_3^- ions. This approach applied to the data of figure 7(*a*) gives a value of $(4 \pm 2) \times 10^{-4}$ for the reactive sticking coefficient of *dry* HNO_3 on NaCl(100) (Laux *et al.* 1994, 1996, Vogt *et al.* 1996). The quoted uncertainty here is dominated by our uncertainty in the thickness of the saturation nitrate film. It is clear from the data of figure 7(*a*) that the reactive sticking coefficient decreases as the reaction proceeds towards saturation. One can also obtain the zero coverage reactive sticking coefficient by fitting the data of figure 7(*a*) to a Langmuir adsorption equation (Somorjai 1981). This is based on the simple assumption that the sticking coefficient is

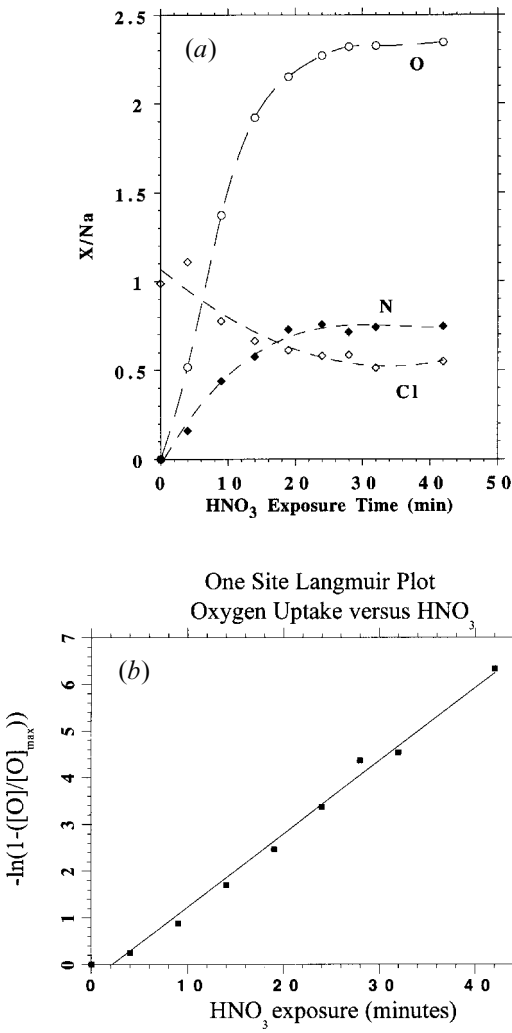

Figure 7. (*a*) O, N and Cl surface concentrations (relative to Na) as a function of dry HNO_3 exposure time for the NaCl(100) surface. The pressure behind the doser capillary was 10 Torr. (*b*) Plot of $\ln(1-([O]/[O]_{max}))$ versus the dry HNO_3 exposure time, where [O] is the oxygen surface concentration shown in (*a*), and $[O]_{max}$ is the high exposure saturation value of the oxygen surface concentration shown in (*a*). The solid line is a linear least squares fit to the data, indicating a good fit to a simple one-site Langmuir adsorption model.

directly proportional to the number of unreacted sites on the surface. If one assumes that each HNO_3 molecule uses up one reactive site, the surface oxygen coverage would be expected to exhibit the following behaviour as a function of HNO_3 exposure time.

$$\ln\left(1-\frac{[O]}{[O]_{max}}\right) = -kt, \tag{7}$$

where [O] and $[O]_{max}$ are the oxygen surface concentrations at time t and at saturation respectively, and k gives the reactive sticking coefficient at zero coverage. Figure 7(*b*) shows such a plot for the oxygen data of figure 7(*a*). Our data are well described by the

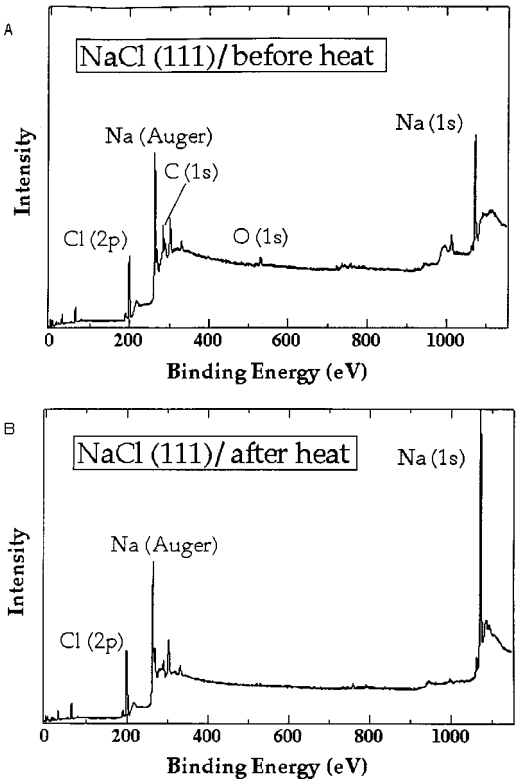

Figure 8. X-ray photoelectron survey spectra of NaCl(111). (*a*) Immediately after pumping the sample down to ultra high vacuum. (*b*) After heating to remove carbon and oxygen containing contaminants.

single site Langmuir adsorption model. This analysis gives a zero coverage reactive sticking coefficient for HNO_3 on NaCl of $(1.3 \pm 0.6) \times 10^{-3}$. As is discussed in detail in the adjacent article by Finlayson-Pitts and co-workers (DeHaan *et al.* 1999) and later in this article, our measured value for the reactive sticking coefficient associated with reaction (1) under dry HNO_3 conditions is significantly lower than several reported values obtained on powdered NaCl samples with Knudsen cell and flow techniques. Davies and Cox (1998) using relatively large crystallites in a flow tube experiment have recently reported values similar to our value. They also measured a significant dependence of the reactive sticking coefficient on the HNO_3 pressure. Davies and Cox explain the pressure dependence of their data by invoking a model that requires two sites for reactive sticking of HNO_3. Such a model is inconsistent with the data of figure 7(*a*) which is well fit by a single site model as shown in figure 7(*b*). This will be discussed in some detail later in this article.

As we have discussed, the freshly cleaved NaCl(100) surface is relatively defect free. In contrast if one prepares a NaCl sample with the macroscopic plane parallel to the (111) plane of the bulk, the surface is highly defective. As pointed out earlier, this is because the (111) plane of the bulk NaCl structure contains either all Na^+ ions or all Cl^- ions and as such is electrostatically unstable as a terminating surface layer. The result is that the surface facets, exposing a large number of planes and generating a rough highly defective surface. Figure 8 shows XPS survey spectra of a NaCl(111) surface before and after heating the sample in UHV to $\sim$ 573 K. Figure 8(*a*) shows

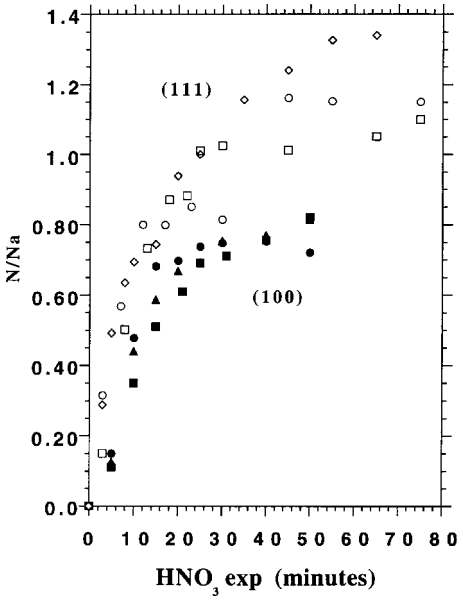

Figure 9. Nitrogen surface concentrations from X-ray photoelectron spectra as a function of dry HNO_3 exposure to the samples. The solid data points were obtained for NaCl(100) samples. The open data points were obtained for NaCl(111) samples. In each case the different symbols indicate completely different experiments on different samples.

that unlike the NaCl(100) surface the NaCl(111) sample which has just been introduced into the vacuum system has measurable contamination in the form of C and O. The binding energy of the O species (531.8 eV) is consistent with a OH^- surface species (Moulder *et al.* 1992). As is shown in figure 8(*b*) heating the sample to 573 K removes these contaminants. Figure 9 compares the results of HNO_3 exposure experiments for the NaCl(111) sample with ones for a NaCl(100) sample (here we plot only the N/Na ratio for clarity). In this set of experiments the pressure of dry HNO_3 behind the doser capillary was 7 Torr, resulting in a comparatively longer saturation time than that shown in the data of figure 7. The different symbols in figure 9 correspond to results from experiments with different samples. The data for the three different NaCl(100) samples agree quite closely. The data for the two different NaCl(111) samples also agree well, with some scatter at long times. However, there is clearly a systematic difference between the results for the NaCl(111) surface and the NaCl(100) surface. The initial slope of the reactive uptake (ϕ) may be slightly larger for the NaCl(111) surfaces compared to the NaCl(100), but this appears to be a minor difference (less than a factor of 2). It appears, however, that the saturation behaviour of the two kinds of surfaces may be different.

4.2. *Water induced recrystallization of $NaNO_3$ ultrathin films (XPS and TEM)*

If, as our experiments indicate, the result of reaction (1) is the formation of a one to two layer thick film of $NaNO_3$ which acts to passivate the surface, then some additional process which acts to break up the $NaNO_3$ film must exist if this chemistry on solid sea salt particles is to contribute significantly to chlorine depletion that has been observed in collected sea salt particles. In light of this we have studied the effect that water vapour has on reaction (1). In these experiments a NaCl(100) sample was exposed to a saturation amount of dry HNO_3 resulting in an ultrathin $NaNO_3$ film.

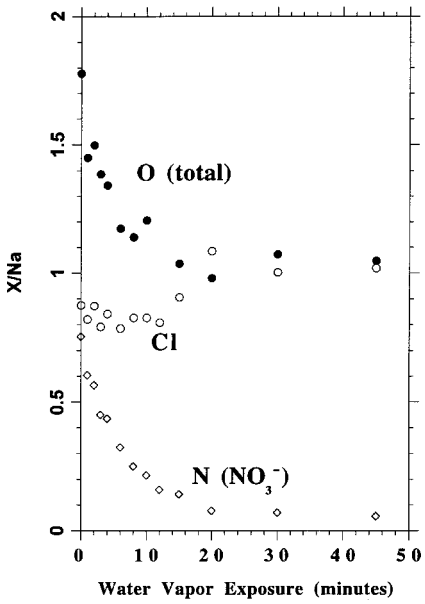

Figure 10. Surface concentrations of O, Cl and N (NO_3^-) versus H_2O exposure time at a H_2O pressure of 2 Torr, following saturation of the NaCl(100) surface with HNO_3(g).

This sample was then exposed to water vapour and the surface composition was monitored as a function of exposure using XPS. Figure 10 shows the Cl 2p and N 1s signals from an experiment in which the water vapour pressure used was 2 Torr. The Cl 2p signal is seen to increase and the N 1s signal decreases as a function of water vapour exposure. While this behaviour could be consistent with a number of models for changes in the surface, TEM experiments (Vogt and Finlayson-Pitts, 1994a, b, 1995, Allen *et al.* 1996) (described below) show that water vapour exposure leads to enhanced ionic mobility in the $NaNO_3$ film and phase separation of the $NaNO_3$ from the NaCl and the growth of three-dimensional crystals of $NaNO_3$. The decrease of the N 1s signal and the increase of the Cl 2p signal are consistent with this. The N 1s signal decreases since the three-dimensional crystals are sufficiently thick that the XPS experiment which is sensitive to only the top few layers of the $NaNO_3$ does not detect all of the $NaNO_3$. The $NaNO_3$ which is internal to the newly formed crystallites is no longer detected by the experiment. As the $NaNO_3$ crystallites grow this leaves uncovered fresh NaCl surface areas, which leads to the observed increase in the Cl 2p signal. After the recrystallization, the surface is no longer passivated towards reaction (1) and subsequent exposure to HNO_3 leads to additional reactivity and the regrowth of the $NaNO_3$ film. This process can be repeated a very large number of times (Laux 1996).

TEM experiments were carried out on NaCl crystallites to determine what the water vapour exposure was doing to the surface of HNO_3 saturated NaCl surfaces. These experiments involved the TEM imaging and identification of micron size NaCl crystallites, followed by exposure to HNO_3, which was followed by exposures to H_2O vapour. The same crystallites where identified and imaged after HNO_3 exposure and then after H_2O vapour exposure. Figure 11 shows TEM images from one such experiment. Figure 11(*a*) shows a NaCl crystallite which is approximately 3 μm across. This crystal was identified as NaCl by electron diffraction in the TEM as well as by X-

Reactions of NaCl and HNO_3 Followed by Exposures to Water Vapor

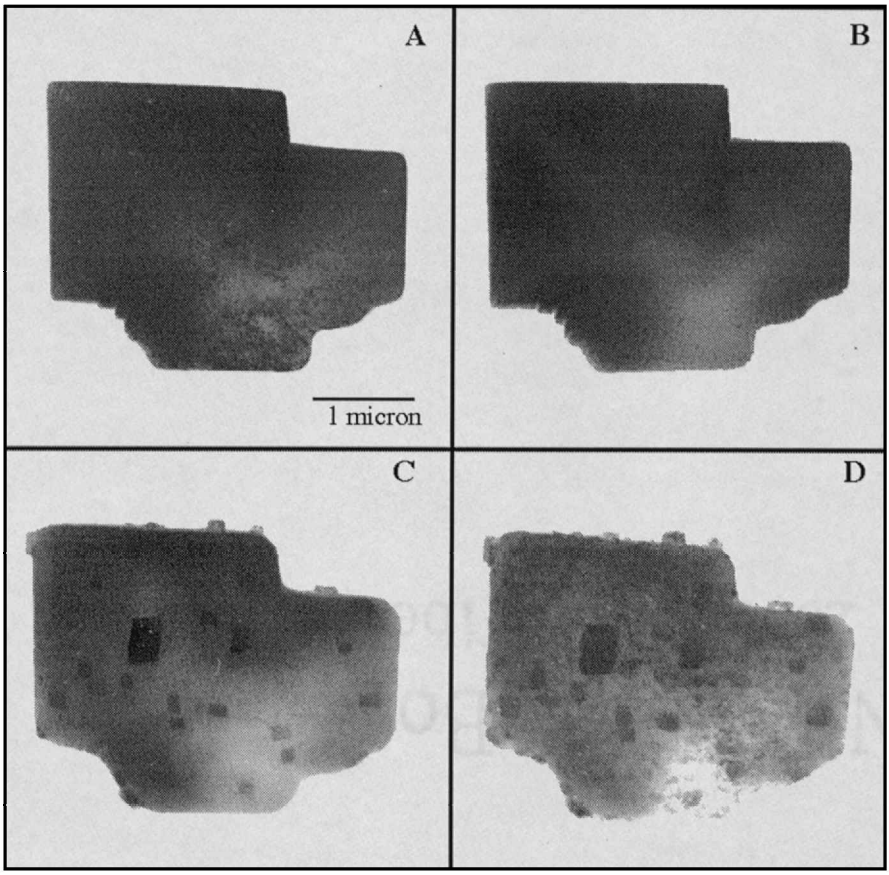

Figure 11. Transmission electron microscope images of a NaCl crystallite. (*a*) Initial crystallite after growth on the TEM grid. (*b*) After exposure of the sample from (*a*) to HNO_3. (*c*) After exposure of the sample from (*b*) to water vapour. (*d*) After exposure of the sample from (*c*) to another sequence of HNO_3 followed by water vapour.

ray fluorescence (Allen 1997). Figure 11(*b*) shows the same crystallite after exposure to HNO_3 vapour. The HNO_3 exposure causes no substantial change in the morphology of the crystal. Based on our XPS experiments the crystal is coated with an ultrathin film of $NaNO_3$ as the result of the reaction with the HNO_3. Figure 11(*c*) shows the crystal after further exposure to H_2O. The crystal is now decorated with many small crystallites. Figure 11(*d*) was obtained after a subsequent cycle of HNO_3 exposure followed by H_2O exposure. As can be readily seen this leads to the growth of additional small crystals.

The crystallites growing on the NaCl crystal are identified as $NaNO_3$ by X-ray fluorescence experiments in the electron microscope (Allen *et al.* 1996). Figure 12 shows the results of X-ray fluorescence experiments carried out on crystallites similar to those shown in figure 11(*c*). Figure 12(*a*) shows the spectrum obtained from a small

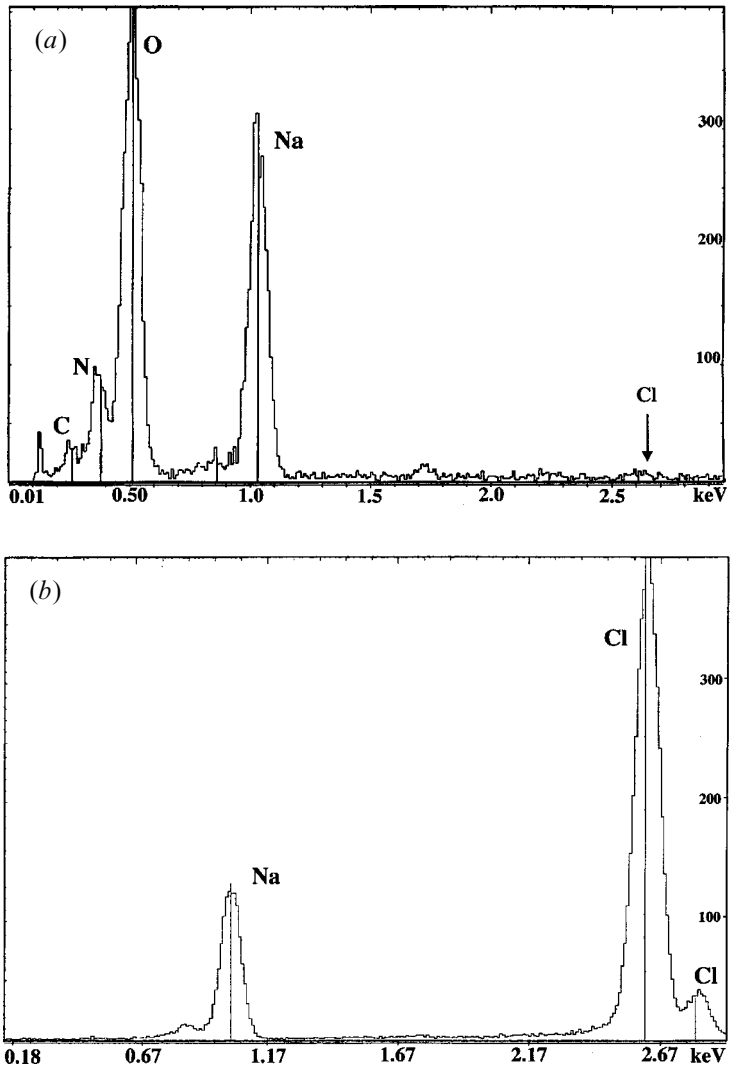

Figure 12. EDS (X-ray fluorescence) spectra. (*a*) Spectrum obtained when the electron beam was focused on a new particle which grew as the result of water exposure to the HNO_3 saturated NaCl crystallite, indicating sodium, nitrogen and oxygen and no chlorine. (*b*) Spectrum obtained after water exposure to the HNO_3 saturated NaCl crystallite but to obtain this spectrum the electron beam was focused on a region of the original crystallite which did not show new particle formation, indicating the expected sodium and chlorine content.

crystallite which was growing off the edge of the host NaCl crystal. This spectrum was obtained by focusing the electron beam on a small crystallite which extended sufficiently away from the NaCl host crystal so that background signals from the host NaCl crystal could be avoided. Na, O and N are all clearly visible in this spectrum. A small amount of carbon signal is also observed from the formvar polymer of the TEM sample grid. Note that the energy in the spectrum where the Cl signal would be expected shows no evidence of Cl in this small crystallite. Figure 12 (*b*) shows the X-ray fluorescence spectrum obtained by focusing the electron beam on the host NaCl crystal. As expected only Na and Cl are observed. Attempts were made to obtain

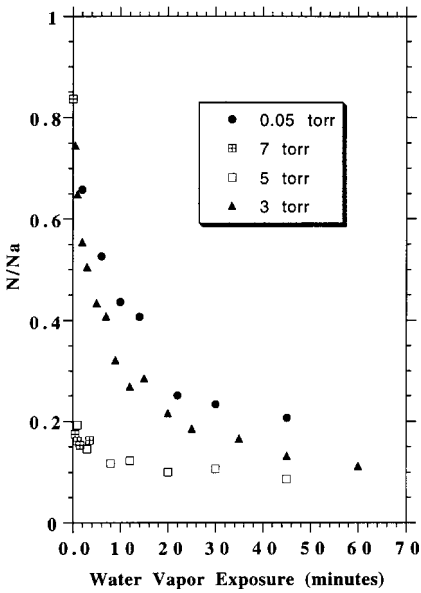

Figure 13. Nitrogen surface concentrations (relative to Na) from N 1s X-ray photoelectron spectra for NaCl(100) surfaces after saturation exposure of dry HNO_3 as a function of water vapour exposure time for a variety of water vapour pressures as indicated.

electron diffraction patterns from the newly formed crystallites, but these very small crystallites proved to be too electron beam sensitive to obtain high quality diffraction patterns (Allen *et al.* 1996, Allen 1997). It is interesting to note however, that the shapes of the $NaNO_3$ crystallites are observed to be non-cubic, which is consistent with the rhombohedral $NaNO_3$ crystal structure.

Since the HNO_3 and H_2O exposures could not be carried out *in situ* in the TEM, it is difficult to quantify the H_2O induced recrystallization with just TEM experiments. However, the TEM experiments explicitly show that the process involved in the changes in the XPS spectra with water exposure is the phase separation and three-dimensional recrystallization of the $NaNO_3$. With this process identified, the XPS experiments can be used to further quantify this phenomena. Figure 13 shows the N 1s signal in experiments in which the NaCl(100) surface was exposed to dry HNO_3 to form the saturated $NaNO_3$ film followed by exposure to water vapour. Figure 13 shows data from four experiments in which different water vapour pressures were used (0.05, 3, 5 and 7 Torr). Even exposure to water vapour pressures as low as 0.05 Torr results in enhanced ionic mobility in the $NaNO_3$ film and recrystallization. This is somewhat surprising since, as mentioned previously, the deliquescence point for $NaNO_3$ at room temperature is $\sim$ 17.5 Torr water vapour. It might be thought that the simplest explanation for water enhanced ionic mobility which leads to the phase separation and recrystallization that we observe would be for the water to cause deliquescence of the $NaNO_3$ ultrathin film. However, it is highly unlikely that the deliquescence behaviour of the $NaNO_3$ covered surface would be so different from that of bulk $NaNO_3$. This will be discussed in more detail in the discussion section of this article.

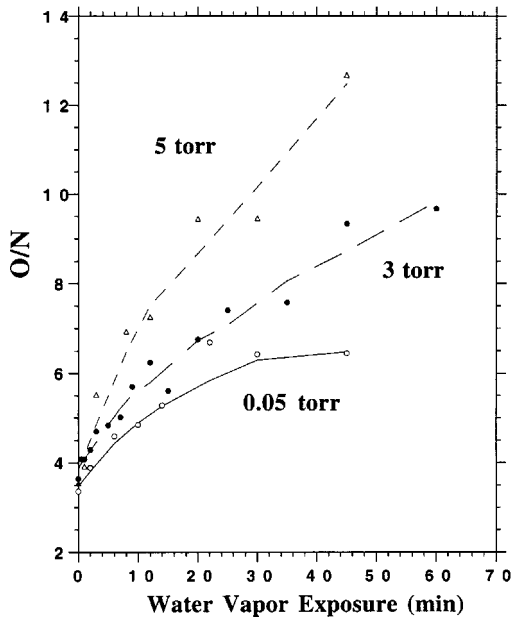

Figure 14. Ratio of the oxygen and nitrogen surface concentrations from O 1s and N 1s X-ray photoelectron spectra for a NaCl(100) sample after exposure to a saturation dose of dry HNO_3 as a function of water vapour exposure time. The water vapour pressure used is indicated in the figure.

4.3. *Dissociative adsorption of water on HNO_3 corroded surfaces*

If the only thing that happens when a $NaNO_3$ coated NaCl(100) surface is exposed to water is the three-dimensional recrystallization of the $NaNO_3$ then one would expect the O/N ratio in the XPS experiments to remain constant at the 3:1 stoichiometry. Figure 14 shows that this is not what is observed. Figure 14 shows the O 1s/N 1s ratios as a function of H_2O exposure for NaCl(100) samples which had been precovered with the saturation $NaNO_3$ film. The data show that the O/N ratio increases dramatically in these experiments. A more detailed examination of the O 1s spectrum shows what is happening in these experiments. Figure 15 shows the O 1s spectra as a function of H_2O exposure for a H_2O pressure of 3 Torr. Prior to any water exposure (0 min spectrum) a single O 1s peak is observed with a binding energy (533.3 eV) consistent with $NaNO_3$. As the sample is exposed to H_2O vapour, the O 1s peak due to $NaNO_3$ decreases as expected. However, there is clearly a new peak growing into the spectrum as a shoulder at lower binding energy. A two peak deconvolution of the 10 min H_2O exposure spectrum is shown in figure 16. The binding energy of the shoulder peak which grows with H_2O exposure is 531.5 eV. This binding energy is consistent with an OH^- species being formed on the surface. By deconvoluting each of the O 1s spectra in figure 15 we can obtain the surface concentration of the two oxygen containing species (OH^- and NO_3^-) as a function of H_2O exposure. Figure 17 shows a plot of the total oxygen signal as well as the signals due to OH^- and NO_3^- as a function of H_2O exposure at 2 Torr. As the total oxygen signal decreases due to the growth of the $NaNO_3$ crystallites, it is seen that the OH^- signal increases substantially.

Using only the deconvoluted NO_3^- oxygen signal and the nitrogen peak areas from this experiment, it is observed that the O:N ratio remains constant at 3:1 over the entire range of H_2O exposure. The O 1s binding energies for NO_3^- and molecularly

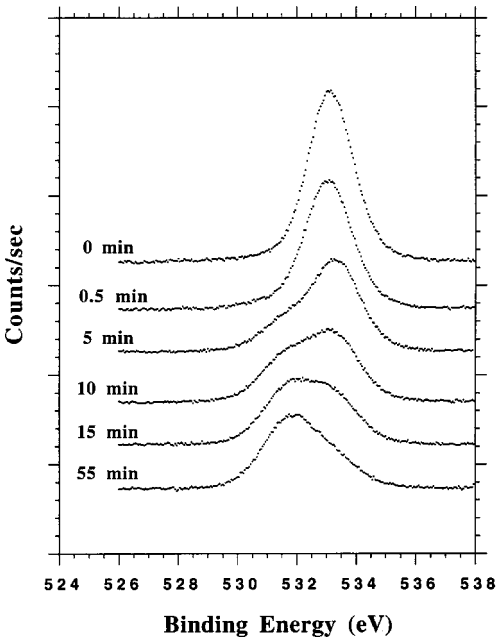

Figure 15. O 1s X-ray photoelectron spectra for a NaCl(100) sample after exposure to a saturation dose of dry HNO_3. The sample was then exposed to 3 Torr of water vapour for the indicated time before the spectrum. The binding energy has been corrected for charging as indicated in the experimental section of the text.

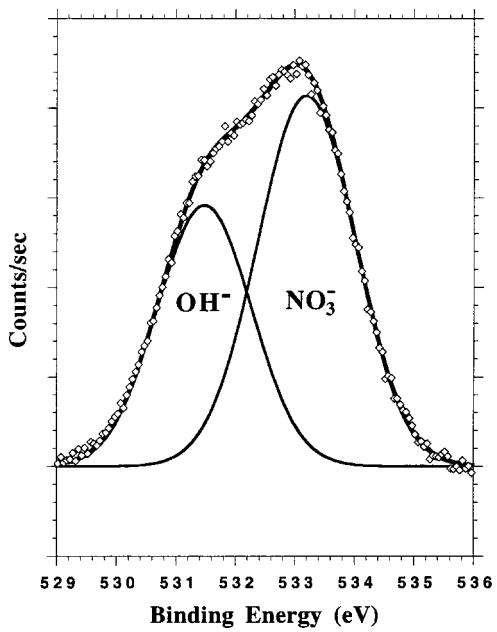

Figure 16. Deconvolution of the O 1s X-ray photoelectron spectra for a NaCl(100) sample after exposure to a saturation dose of dry HNO_3 followed by exposure to 3 Torr of water vapour for 10 min.

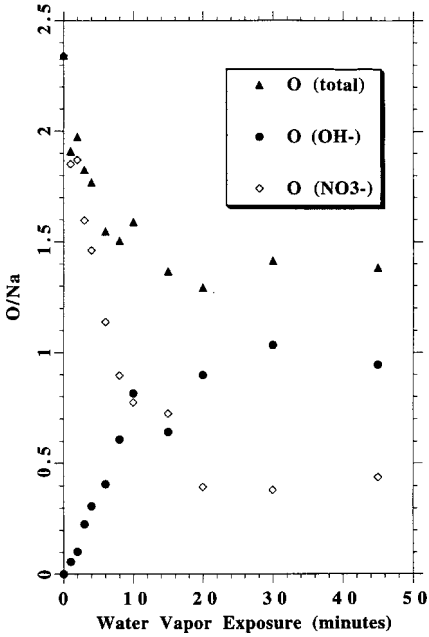

Figure 17. Total oxygen surface concentration (relative to sodium), and the oxygen surface concentration due to OH^-, and NO_3^- for a NaCl(100) sample exposed to a saturation dose of dry HNO_3 plotted as a function of the subsequent water vapour exposure time at a water vapour pressure of 2 Torr. The OH^- and NO_3^- surface concentrations were obtained by deconvoluting the spectra similar to those shown in figure 15 in the same manner as is illustrated in figure 16.

adsorbed water are expected to be quite similar. Thus from a simple examination of the spectra in figure 15 we cannot rule out the adsorption of some molecular water. However, the fact that the ratio of the O 1s peak at 533.3 eV to the N 1s peak remains at 3:1 indicates that this oxygen is predominantly due to residual signal from the NO_3^- species. Thus, it is clear that under the UHV, room temperature conditions used in these experiments there is no molecularly adsorbed water on the surface. As discussed before, this is consistent with what is known about water adsorption on NaCl(100). The details of water adsorption on the surfaces of $NaNO_3$ is, however, less well studied. Our experiments provide good evidence that, similar to NaCl(100), $NaNO_3$ does not molecularly adsorb water at room temperature. As mentioned earlier, there is evidence (both experimental and theoretical) for the dissociative adsorption of water at defect sites on NaCl surfaces and clusters (Dai *et al.* 1995, Barnett and Landman 1996, Taylor *et al.* 1997). Thus, it is possible that the corrosion of the NaCl(100) surface by the combined action of HNO_3 and H_2O leaves a highly defective surface, and that this is where the dissociative adsorption of water is occurring. However, it is important to remember that we know little of the detailed chemistry of $NaNO_3$ surfaces, and it is possible that a defect free $NaNO_3$ surface could dissociatively adsorb water. This issue remains to be investigated.

5. Discussion

The experiments on structurally controlled surfaces which have been described here have resulted in a number of new insights into the chemistry of HNO_3(g) with NaCl(s).

(1) Dry HNO_3(g) reacts with defect free NaCl(100) to form $NaNO_3$(s) with a zero coverage reactive sticking coefficient of $(1.3 \pm 0.6) \times 10^{-3}$.
(2) The reaction of *dry* HNO_3 with NaCl(100) is well fit by a single-site Langmuir adsorption model and saturates after the formation of a passivating $NaNO_3$(s) film which is 1–2 layers thick.
(3) Water vapour exposure to the passivating $NaNO_3$(s) film results in enhanced ionic mobility which leads to phase separation and three-dimensional recrystallization of the $NaNO_3$(s) leaving open areas of NaCl(s) for further reaction.
(4) The vapour pressure of water required to generate the enhanced ionic mobility is surprisingly low ($\leqslant 0.05$ Torr).
(5) The HNO_3 and H_2O corroded NaCl surface is active for the dissociative adsorption of water to form surface OH^-.
(6) The reaction of *dry* HNO_3 on the highly defective NaCl(111) proceeds with a similar reaction probability to that on the NaCl(100) surface but it does not appear to form a passivating $NaNO_3$ film.

5.1. *Water induced recrystallization of metastable $NaNO_3$ films*

One of the most dramatic results presented here is the fact that exposure to H_2O vapour pressures as low as 0.05 Torr can increase the ionic mobility in the $NaNO_3$ film to an extent that macroscopic recrystallization of the film is possible. It is possible that surface deliquescence may occur at a lower vapour pressure than deliquescence of the bulk. However, recent atomic force microscopy experiments by Xu *et al.* (1998) (polarization contrast mode) and Shindo *et al.* (1996) show that the surface mobility as a result of water vapour exposure on NaCl(100) surfaces does not become significant until water vapour pressures quite close to the bulk deliquescence point. While $NaNO_3$ may differ from NaCl in this property, it is unlikely that the 'surface' deliquescence would be so different from the bulk. A more likely explanation for the enhanced ionic mobility that we observe at low water vapour pressure lies in the structure of the $NaNO_3$ film that is formed when HNO_3 is reacted with NaCl(100). Both the XPS and X-ray fluorescence experiments described in this article show that the reaction of dry HNO_3 with NaCl(100) results in a solid product with the stoichiometry of $NaNO_3$. However, other than knowing that the film that is formed provides a passivating film for the surface, we have no experimental evidence regarding the structure of the film. It is, however, clear that in the absence of water there is very little ionic mobility as the reaction proceeds. Thus, it seems reasonable to view the reaction as a simple ion exchange reaction in which Cl^- ions in the NaCl surface are replaced with NO_3^- ions with little or no restructuring of the surface. If this is the case, then the initial solid phase product of reaction (1) is a film with the stoichiometry $NaNO_3$ (in agreement with XPS experiments) but with the NaCl(100) structure. Since the stable crystal structure of bulk $NaNO_3$ is rhombohedral, this suggests that the initially formed $NaNO_3$ film is generated as a structurally metastable phase. Such an interpretation of our results is also consistent with diffuse reflectance infrared spectroscopy studies which Finlayson-Pitts and co-worker have carried out on powdered NaCl samples (Vogt and Finlayson-Pitts 1994a, b). In those experiments they observed that the initial solid phase products of reaction (1) had an infrared spectrum with bands in the NO_3^- region but with an unexpected lineshape. Following water exposure, the lineshape converted to that of bulk $NaNO_3$. Our interpretation would assign the initial infrared spectra to that of stoichiometric $NaNO_3$ in a NaCl

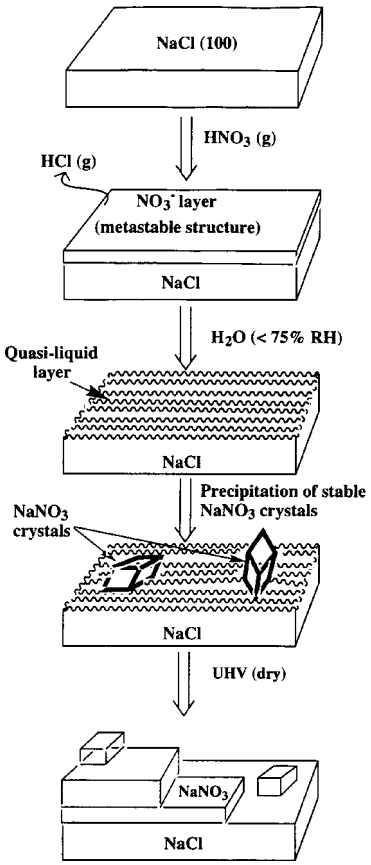

Figure 18. Schematic model of the phenomena which occur when a NaCl(100) sample is exposed to HNO_3 vapour followed by H_2O vapour. The HNO_3 exposure leads to the formation of a metastable surface layer of $NaNO_3$ stoichiometry followed by the water induced enhancement of the surface ionic mobility leading to recrystallization of the $NaNO_3$ into three-dimensional crystallites leaving open NaCl surface for further reaction.

structure followed by recrystallization to the rhombohedral $NaNO_3$ structure upon water exposure. The surface free energy of the $NaNO_3$ film in the metastable NaCl structure would be expected to be substantially higher than that for the surface of $NaNO_3$ in the stable rhombohedral structure. The higher surface free energy of the initially formed $NaNO_3$ could provide the driving force for 'deliquescence' or ionic mobility at lower than expected water vapour pressures. We refer to this as the formation of a 'quasi-liquid' layer. Since, based on our XPS measurements, we know that the $NaNO_3$ film is at most two layers thick, we prefer to distinguish between this situation and a true $NaNO_3$ solution. Once the ionic mobility is increased there would be a clear free energy driving force for the 'precipitation' of three-dimensional crystals of $NaNO_3$ in the stable rhombohedral structure, as we have observed in our TEM experiments. Figure 18 summarizes the several stages the system goes through as NaCl(100) is exposed first to dry HNO_3 followed by water exposure and eventually to examination in ultra-high vacuum.

5.2. *Dissociative adsorption of water on HNO_3/H_2O corroded NaCl surfaces*

XPS experiments as a function of water exposure after reaction (1) has been run to saturation with dry HNO_3 on NaCl(100) clearly show dissociative adsorption of water with the formation of surface OH^-. This is in stark contrast to the behaviour of water adsorption on defect free NaCl(100) surfaces where water adsorption is completely reversible and water only remains on the surface at temperatures below ~ 150 K. At water vapour pressures below $\sim 50\%$ of the bulk deliquescence point, where the Na^+ and Cl^- ions do not appear to be mobile, it is likely that the corrosion of the NaCl(100) surface by exposure to dry HNO_3 followed by water vapour leaves the surface severely pitted in addition to the decoration with $NaNO_3$ crystallites as shown by the TEM experiments. Thus, the surface is expected to contain reasonable concentrations of defect sites. Although the identity of sites which are active for water dissociation are not known in detail, it has been shown that surface defects can lead to the dissociative adsorption of water with OH^- as the product (Dai *et al.* 1995). The existence of substantial concentrations of surface OH^- could have a dramatic impact on the reactivity of the surface. As has been shown by Henzler and co-workers (Fölsch and Henzler 1991, Fölsch *et al.* 1992) surface OH^- on defective NaCl surfaces can lead to enhanced binding of molecular water. As described in detail in the adjacent article by Finlayson-Pitts and co-workers (DeHaan *et al.* 1999), experiments in their laboratory have demonstrated the existence of 'strongly adsorbed water' (SAW) on NaCl powders. This water species, which is stable on the surface following heating to 343 K in vacuum overnight is active in the reaction of HNO_3 with such surfaces. It is possible that clustering of water around significant concentrations of surface OH^- could be the cause of this SAW. It should be noted, that Henzler and co-workers (Fölsch and Henzler 1991, Fölsch *et al.* 1992) did observe strong interactions between isolated OH^- species and water resulting in stable adsorption of water on NaCl at temperatures above that observed for defect free clean NaCl. Their experiments were, however, conducted at lower temperatures than those described here (they identified water adsorption on a surface with isolated OH^- species at ~ 160 K, whereas the surface of clean, defect free NaCl(100) had to be cooled to 140 K for them to observe water adsorption).

5.3. *Comparison between UHV experiments and Knudsen cell and flow reactor experiments, and the HNO_3 pressure dependence of the reactive sticking coefficient*

Our UHV experiments provide a reaction probability for the well defined reaction system of dry HNO_3 reacting with the clean NaCl(100) surface of $(1.3 \pm 0.6) \times 10^{-3}$. This is substantially smaller than the value reported by several laboratories using Knudsen cell and flow reactor techniques (Leu *et al.* 1995, Beichert and Finlayson-Pitts 1996, Fenter *et al.* 1996) which are in good agreement at $\sim (1-2) \times 10^{-2}$. Based on experiments by Finlayson-Pitts and co-workers (DeHaan *et al.* 1999), it is clear that strongly adsorbed water on the powdered samples plays a crucial role in the chemistry. Based on our results showing the water enhanced recrystallization phenomena, this is not at all surprising.

It should also be noted that the flow reactor studies of Leu *et al.* (1995) showed a substantial HNO_3 pressure dependence to the reaction probability. The reaction probability that they report of $\sim 10^{-2}$ which is in agreement with Knudsen cell measurements, was measured at a HNO_3 pressure of $\sim 10^{-8}$ Torr. Flow reactor experiments that they carried out at higher pressures apparently provide substantially lower reaction probabilities, in closer agreement with our experiments. The UHV

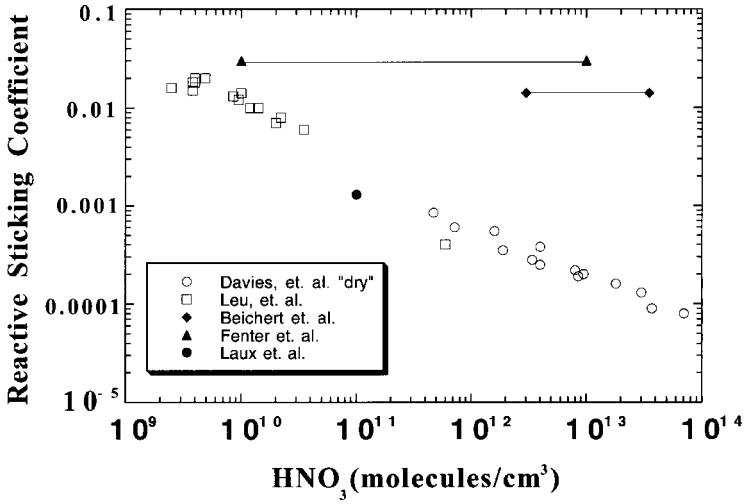

Figure 19. Measured values of the reactive sticking coefficient for HNO_3 on NaCl from a number of different laboratories (literature references indicated in the insert) as a function of HNO_3 gas phase concentration. Beichert and Finlayson-Pitts (1996) and Fenter *et al.* (1996) report values which were observed to be independent of HNO_3 gas phase concentration over the ranges indicated by the horizontal lines.

doser experiments reported here utilize pressures equivalent to $\sim 10^{-6}$ Torr, which is closer to that of a polluted atmosphere. In the experiments with dry HNO_3 we would not expect to see a pressure dependence to the reaction probability. However, in the case of reactions on the 'wet' powdered samples used in Knudsen cells and flow reactors our present picture involves a complex surface which is restructuring as the reaction happens. Depending on the detailed kinetics the surface restructuring may become rate limiting under higher reactant pressures and one may approach conditions in the flow reactor experiments in which the reaction partially passivates the surface.

Figure 19 shows the numbers for the reactive sticking coefficient of HNO_3 on NaCl taken from the literature plotted against the HNO_3 pressure. It is important to recognize that all of the Knudsen cell and flow reactor values are obtained from experiments running under *steady state* reaction conditions. Based on our present understanding of the lack of mobility of the $NaNO_3$ reaction product under dry conditions, it is clear that adsorbed water is required to obtain steady state reaction conditions. The Knudsen cell experiments of Fenter *et al.* (1996) and Beichert and Finlayson-Pitts (1996) are in reasonable agreement and show no HNO_3 pressure dependence. In the flow reactor experiments of Leu *et al.* (1995) and of Davies and Cox (1998) the reactive sticking coefficients exhibit a substantial HNO_3 pressure dependence. In addition, Davies and Cox show that the absolute value of the reactive sticking coefficient and the pressure dependence they observe depends on the H_2O vapour pressure in the flow stream. The NaCl samples used in the Davies and Cox flow reactor experiments were large crystallites (~ 0.5 mm in size). We have shown that such large crystallites typically have substantially smaller amounts of strongly adsorbed water than do the small crystallites typically used in the Knudsen cell experiments (Ghosal and Hemminger 1999). Davies and Cox (1998) present a model, to explain their results, that relies on requiring two sites for the dissociative adsorption of HNO_3 on NaCl. The justification of a two-site adsorption model is that two sites are

required to accommodate the two products of the dissociative adsorption (NO_3^- and H_3O^+). Within a Langmuir adsorption model, the two site requirement leads to an approximate $[HNO_3]^{-0.5}$ dependence of the reactive sticking coefficient on the HNO_3 pressure. The $[HNO_3]^{-0.5}$ dependence provides a good fit to the Davies and Cox data. As discussed earlier, however, we have shown that the dissociative adsorption of HNO_3 on NaCl(100) is well described by a one-site Langmuir adsorption model. It is also highly unlikely that the H^+ (or H_3O^+) formed in the dissociative adsorption would be sufficiently immobile to act in a site-blocking capacity. We have proposed (Ghosal and Hemminger 1999) that the observed HNO_3 pressure dependence not due to a two site requirement for dissociative adsorption of HNO_3 but rather is due to the competition between the single-site dissociative adsorption of HNO_3 and the subsequent water induced reorganization of the nitrate product to produce new sites for further reaction. A simple representation of this model is given by the following two reactions.

$$HNO_3 + \text{NaCl Site} = NO_3^-(\text{ads}) + HCl, \tag{8}$$

$$NO_3^-(\text{ads}) + H_2O(\text{ads}) = \text{NaCl Site} + NaNO_3 \tag{9}$$

where NaCl Site represents a surface site which is open for reaction, and NO_3^- (ads) represents a surface nitrate species which is immobile and has blocked the original reactive site. The second reaction indicates that the original reactive site can be regenerated in the presence of adsorbed water which acts to increase the nitrate mobility. At this point we should acknowledge that we do not quantitatively know how much water is required on the surface to mobilize the NO_3^- (ads) species. That is, the stoichiometry of the second reaction with respect to H_2O may be something other than unity. Indeed, it is likely that this process is more complex then we have represented here. With that in mind however, this model does provide a description of the HNO_3 pressure dependence of the reaction which is also consistent with the three major things that have been learned about this system:

(1) that the dissociative adsorption of HNO_3 on solid NaCl follows a one-site Langmuir adsorption model;
(2) that the initial nitrate formed on the surface blocks subsequent reactions;
(3) that water enhances the mobility of the nitrate opening up blocked sites for further reaction.

Under steady-state reaction conditions, reactions (8) and (9) lead to the following relationship between the reactive sticking coefficient (γ), the HNO_3 pressure and the H_2O (ads) concentration (Ghosal and Hemminger 1999).

$$\gamma = k_r A \left\{ \frac{B[H_2O]}{[HNO_3] + B[H_2O]} \right\}, \tag{10}$$

where A is the total number of surface sites (open + blocked), k_r is the rate constant for the dissociative adsorption reaction (reaction (8)) and $B = 4k_m/k_r s$, with k_m the rate constant for the mobilization of NO_3(ads) (reaction (9)) and s is the mean speed of the HNO_3 molecule in the gas phase. Equation (10) indicates that for reactions run under constant water vapour pressures a plot of γ versus $C/([HNO_3] + C)$ should be linear, with a slope equal to the $k_r A$. Figure 20 shows that a very good fit to the HNO_3 pressure dependent data of Davies and Cox is obtained with this model.

The maximum value of the reactive sticking coefficient that can be obtained from the model of equations (8) and (9), occurs in the limit of high H_2O (ads)

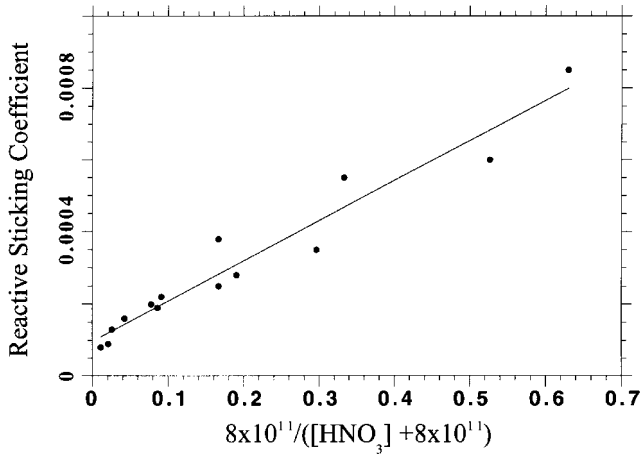

Figure 20. Plot of the reactive sticking coefficient for HNO_3 on NaCl particles (~ 0.5 mm) measured by Davies and Cox (1998) as a function of $C/(\text{nitric acid} + C)$. The constant $C = 8.0 \times 10^{11}$ was chosen to obtain the best linear least squares fit to the data. This functional behaviour of the reactive sticking coefficient on the HNO_3 gas phase concentration is suggested by the model described in the text.

concentrations, when the reaction is not limited by the site blocking of NO_3^- (ads). Under such conditions, the maximum value of γ is given by the slope of the plot in figure 20.

$$\gamma_{max} = 1.1 \times 10^{-3}.$$

This value is in excellent agreement with our measured value, using NaCl(100) single crystals, for the zero coverage value of γ of $(1.3 \pm 0.6) \times 10^{-3}$. It should also be noted that the model of equations (8) and (9) would predict that under conditions of high adsorbed water concentration the value of γ would be independent of the HNO_3 pressure. The model just presented describes well the data for the NaCl(100) experiments and the experiments of Davies and Cox (1998) on relatively large crystallites. However, the maximum value of γ of 1.1×10^{-3} is still significantly lower than the values reported by Fenter *et al.* (1996) and Beichert and Finlayson-Pitts (1996). Both of those experiments utilized substantially smaller crystallites which might have more defects and as a result more adsorbed water. A fundamental description of the origin of these differences is still needed.

There are also issues associated with sample surface area that need to be addressed for the powdered NaCl experiments. Attempts have been made to estimate the 'effective' surface area for a powdered sample in a flow reactor or Knudsen cell, using porosity models, but many of the reaction probabilities, obtained from Knudsen cell measurements reported in the literature, are based on an assumption that the geometrical surface area of the powdered sample is the reactive surface. Once again the resolution of this may be related to the behaviour of surface water in such samples.

6. Conclusions

It is becoming increasingly clear that reactions of sea salt particles in the marine troposphere are an important source of active halogenated compounds. The reactions of gaseous species such as nitrogen oxides with the surfaces of sea salt particles are clearly complex on a molecular level of detail. The importance of adsorbed water to the surface ionic mobility and the subsequent morphological changes that occur

during the reaction have been made clear by UHV surface science studies of the fundamental processes involved as well as by the detailed Knudsen cell measurements of the reaction rates and infrared spectroscopy studies of surface reaction intermediates on powdered samples. While there has been significant progress in our understanding of this complex system, we are only beginning to understand the detailed chemistry at a molecular level. The relatively simple model described in equations (8) and (9) explains the observed experimental results on single crystals and larger crystallites, where the water content is limited. A detailed understanding of the strongly adsorbed water that is observed on defective surfaces such as NaCl(111) and powdered samples is still not complete. A detailed molecular level description of these phenomena is critical to provide an accurate quantitative assessment of the impact of the chemistry of sea salt particles in the marine troposphere.

Acknowledgments

The work described in this article was supported by the National Science Foundation. Most of the data described here has been the work of talented students and postdoctorals, including Mickey Laux, Dr Thomas Fister, and Sutapa Ghosal on the XPS experiments and Heather Allen on the TEM experiments. Collaborations with the research scientists in the Finlayson-Pitts research group, in particular Dr Rainer Vogt, were critical to our experimental successes. Many thanks go to Barbara Finlayson-Pitts for introducing us to the excitement of atmospheric chemistry and in particular to the importance of problems such as those which are described in this article. Helpful discussions with George Ewing, Barbara Finlayson-Pitts, James N. Pitts Jr and Rainer Vogt, are gratefully acknowledged.

References

ALLEN, H. C., 1997, Fundamental surface processes in heterogeneous atmospheric chemistry: applications to sea-salt (NaCl) and oxide particulate chemistry. PhD dissertation, Department of Chemistry, University of California, Irvine, CA 92697, USA.

ALLEN, H. C., LAUX, J. M., VOGT, R., FINLAYSON-PITTS, B. J., and HEMMINGER, J. C., 1996, *J. phys. Chem.*, **100**, 6371.

ALLEN, H. C., MECARTNEY, M. L., and HEMMINGER, J. C., 1998, *Microsc. Microanal.*, **4**, 23.

BARNETT, R. N., and LANDMAN, U., 1996, *J. phys. Chem.*, **100**, 13950.

BARRACLOUGH, P. B., and HALL, P. G., 1974, *Surf. Sci.*, **46**, 393.

BEICHERT, P., and FINLAYSON-PITTS, B. J., 1996, *J. phys. Chem.*, **100**, 15218.

BENEDEK, G., BRUSDEYLINS, G., DOAK, R., SKOFRONICK, J., and TOENNIES, P., 1983, *Phys. Rev. B*, **28**, 2104.

BLANCHARD, D. C., 1985, *J. Geophys. Res.*, **90**, 961.

BRIGGS, S., and SEAH, M. P., 1990, *Practical Surface Analysis* (New York: Wiley).

BRUCH, L. W., GLEBOV, A., TOENNIES, J. P., and WEISS, H., 1995, *J. chem. Phys.*, **103**, 5109.

CAHILL, T. A., WILKINSON, K., and SCHNELL, R., 1992, *J. Geophys. Res.*, **97**, 14513.

COFER III, W. R., STEVENS, R. K., WINSTEAD, E. L., PINTO, J. P., SEBACHER, D. I., ABDUL-RAHEEM, M. Y., AL-SAHAFI, M., MAZUREK, M. A., RASMUSSEN, R. A., CAHOON, D. R., and LEVINE, J. S., 1992, *J. Geophys. Res.*, **97**, 14521.

DAI, D. J., PETERS, S. J., and EWING, G. E., 1995, *J. phys. Chem.*, **99**, 10299.

DAUM, P. H., AL-SUNARD, A., BUSNESS, K. M., HALES, J. M., and MAZUREK, M. A., 1993, *J. Geophys. Res.*, **98**, 16809.

DAVIES, J. A., and COX, R. A., 1998, *J. phys. Chem. A*, **102**, 7631.

DEHAAN, D. O., BRAUERS, T., OUM, K., STUTZ, J., NORDMEYER, T., and FINLAYSON-PITTS, B. J., 1999, *Int. Rev. phys. Chem.*, **18**, 343.

EVELYN, J., 1661, *Fumifugium: or, The Inconvenience of the Aer and Smoak of London Dissipated, Together with some Remedies Humbly Proposed* (London: Bedel and Collins).

EWING, G. E., 1991, *Int. Rev. phys. Chem.*, **10**, 391.

EWING, G. E., and PETERS, S. J., 1997, *Surf. Rev. Lett.*, **4**, 757.
FENTER, F. F., CALOZ, F., and ROSSI, M. J., 1996, *J. phys. Chem.*, **100**, 1008.
FEREK, R. S., HOBBS, P. V., HERING, J. A., LAURSEN, K. K., WEISS, R. E., and RAMUSSEN, R. A., 1992, *J. Geophys. Res.*, **97**, 14483.
FINLAYSON-PITTS, B. J., and PITTS JR, J. N., 1986, *Atmospheric Chemistry: Fundamentals and Experimental Techniques* (New York: Wiley).
FÖLSCH, S., and HENZLER, M., 1991, *Surf. Sci.*, **247**, 269.
FÖLSCH, S., STOCK, A., and HENZLER, M., 1992, *Surf. Sci.*, **264**, 65.
GHOSAL, S., and HEMMINGER, J. C., 1999, *J. phys. Chem.* A, **103**, 4777.
GONG, S. L., and BARRIE, L. A., 1997, *J. Geophys. Res.*, **102**, 3805.
GONG, S. L., BARRIE, L. A., PROSPERO, J. M., SAVOIE, D. L., AYERS, G. P., BLANCHET, J.-P., and SPACEK, L., 1997, *J. Geophys. Res.*, **102**, 3819.
HEBESTRECT, K., STUTZ, J., LURIA, M., PELEG, M., MATVEIV, V., ROZEN, D., and PLATT, U., 1998, *Ann. Geophys. Suppl. II*, **16**, C719.
IKEGAMI, M., OKADA, K., ZAIZEN, Y., and MAKINO, Y., 1994, *Tellus*, **46B**, 142.
JUNGE, C. E., 1956, *Tellus*, **8**, 127.
KEENE, W. C., PSZENNY, A. A. P., JACOB, D. J., DUCE, R. A., GALLOWAY, J. N., SCHULTZ-TOKOS, J. J., SIEVERING, H., and BOATMAN, J. F., 1990, *Global Biogeochem. Cycles*, **4**, 407.
KNUTSEN, K., and ORLANDO, T. M., 1996, *Surf. Sci.*, **348**, 143.
LAUX, J. M., 1996, X-ray photoelectron spectroscopy studies of the reaction of nitric acid and sodium chloride: effects of water, surface defects, and X-rays. PhD dissertation, Department of Chemistry, University of California, Irvine, CA 92697, USA.
LAUX, J. M., FISTER, T. F., FINLAYSON-PITTS, B. J., and HEMMINGER, J. C., 1996, *J. phys. Chem.*, **100**, 19891.
LAUX, J. M., HEMMINGER, J. C., and FINLAYSON-PITTS, B. J., 1994, *Geophys. Res. Lett.*, **21**, 1623.
LEU, M.-T., TIMONEN, R. S., KEYSER, L. F., and YUNG, Y. L., 1995, *J. phys. Chem.*, **99**, 13203.
LINDQUIST, J. M., and HEMMINGER, J. C., 1987, *J. Vac. Sci. Tech. A*, **5**, 118.
LOWENTHAL, D. H., BORYS, R. D., ROGERS, C. F., CHOW, J. C., STEVENS, R. K., PINTO, J. P., and ONDOV, J. M., 1993, *Geophys. Res. Lett.*, **20**, 691.
MCINNES, L. M., COVERT, D. S., QUINN, P. K., and GERMANI, M. S., 1994, *J. Geophys. Res.*, **99**, 8257.
MEYER, G. D., and AMER, N. M., 1990a, *Appl. Phys. Lett.*, **56**, 2100; 1990b, *Appl. Phys. Lett.*, **57**, 2089.
MOULDER, J. F., STICKLE, W. F., SOBOL, P. E., and BOMBEN, K. D., 1992, *Handbook of X-ray Photoelectron Spectroscopy* (Eden, Prairie, MN: Physical Electronics Division, Perkin Elmer Corp.).
MOURI, H., and OKADA, K., 1993, *Geophys. Res. Lett.*, **20**, 49.
MOYERS, J. L., and DUCE, R. A., 1972, *J. Geophys. Res.*, **77**, 5330.
O'DOWD, C. D., SMITH, M. H., CONSTERDINE, I. E., and LOWE, J. A., 1997, *Atmos. Environ.*, **31**, 73.
PARUNGO, F., KOPCEWISZ, B., NAGAMOTO, C., SCHNELL, R., SHEERIDAN, P., ZHU, C., and HARUS, J., 1992, *J. Geophys. Res.*, **97**, 15867.
PETERS, S. J., and EWING, G. E., 1997, *Langmuir*, **13**, 6345.
POSFAI, M., ANDERSON, J. R., BUSECK, P. R., and SIEVERING, H. M., 1995, *J. Geophys. Res.*, **100**, 23063.
REID, J. S., FLOCCHINC, R. G., CAHILL, T. A., and RUTH, R. S., 1994, *Atmos. Environ.*, **28**, 1699.
SHERIDAN, P. J., SCHNELL, R. C., HOFMANN, D. J., HARRIS, J. M., and DESHLER, T., 1992, *Geophys. Res. Lett.*, **19**, 389.
SHINDO, H., OHASHI, M., BABA, M., and SEO, A., 1996, *Surf. Sci.*, **357**, 111.
SOMORJAI, G. A., 1981, *Chemistry in Two Dimensions: Surfaces* (Ithaca, New York: Cornell University Press).
STEVENS, R., PINTO, J., MAMANE, Y., ONDOV, J., ABDULRAHEEM, M., AL-MAJED, N., SADEK, J., COFER, W., ELLENSON, W., and KELLOGG, R., 1993, *Water Sci. Tech.*, **27**, 223.
THIEL, P. A., and MADEY, T. E., 1987, *Surf. Sci. Rep.*, **7**, 211.
TAYLOR, D. P., HESS, W. P., and MCCARTHY, M. I., 1997, *J. phys. Chem.* B, **101**, 7455.
VOGT, R., ELLIOTT, H., ALLEN, H. C., LAUX, J. M., HEMMINGER, J. C., and FINLAYSON-PITTS, B. J., 1996, *Atmos. Environ.*, **30**, 1729.

VOGT, R., and FINLAYSON-PITTS, B. J., 1994a, *J. phys. Chem.*, **98**, 3747; 1994b, *Geophys. Res. Lett.*, **21**, 2291; 1995, *J. phys. Chem.*, **99**, 13052.
WAGNER, C. D., DAVIS, L. E., ZELLER, M. V., TAYLOR, J. A., RAYMOND, R. H., and GALE, L. H., 1981, *Surf. Inter. Anal.*, **3**, 211.
WASSERMANN, B., MIRBT, S., REIF, J., ZINK, J. C., and MATTHIAS, E., 1993, *J. chem. Phys.*, **98**, 10049.
WEISS, H., 1995, *Surf. Sci.*, **331–333**, 1453.
WOODCOCK, A. H., 1953, *J. Meteorol.*, **10**, 362; 1972, *J. Geophys. Res.*, **77**, 5316.
WOODS, D. C., and CHUAN, R. L., 1983, *Geophys. Res. Lett.*, **10**, 1041.
WOODS, D. C., CHUAN, R. L., and ROSE, W. I. 1985, *Science*, **230**, 170.
XU, L., BLUHM, H., and SALMERON, M., 1998, *Surf. Sci.*, **407**, 251.
YATES JR, J. T., 1998, *Experimental Innovations in Surface Science: A Guide to Practical Laboratory Methods and Instruments* (New York: Springer-Verlag Inc.).